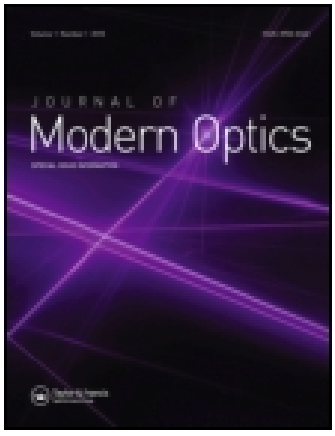

Journal of Modern Optics
Publication details, including instructions for authors and subscription information:
http://www.tandfonline.com/loi/tmop20

Wide-window angular spectrum method for optical field propagation through ABCD systems

Yuanyang Li[ab], Jin Guo[a], Lisheng Liu[a], Tingfeng Wang[a] & Junfeng Shao[ab]
[a] State Key Laboratory of Laser Interaction with Matter, Changchun Institute of Optics, Fine Mechanics and Physics, Chinese Academy of Sciences, Changchun, China
[b] University of Chinese Academy of Sciences, Beijing, China
Published online: 30 Jul 2014.

Journal of Modern Optics, 2014
Vol. 61, No. 18, 1519–1528, http://dx.doi.org/10.1080/09500340.2014.944232

Wide-window angular spectrum method for optical field propagation through ABCD systems

Yuanyang Li[a,b]*, Jin Guo[a], Lisheng Liu[a], Tingfeng Wang[a] and Junfeng Shao[a,b]

[a]*State Key Laboratory of Laser Interaction with Matter, Changchun Institute of Optics, Fine Mechanics and Physics, Chinese Academy of Sciences, Changchun, China;* [b]*University of Chinese Academy of Sciences, Beijing, China*

(*Received 6 March 2014; accepted 8 July 2014*)

The wide-window angular spectrum (WWAS) method is proposed to simulate field propagation through paraxial optical systems, mainly based on the Collins formula and the scaled Fourier transform (SFT). The application of the SFT algorithm makes the sampling processes in the input space, output space and spatial-frequency domains completely independent, and as a result, we can choose a larger calculation window size for simulating long-distance propagation without increasing the calculation burden. The sampling criteria are derived analytically and used in the numerical simulations to present the correctness and effectiveness of the WWAS algorithm. The advantages of the algorithm are shown by making a comparison with other angular spectrum methods for the free-space propagation case.

Keywords: field propagation; paraxial optical systems; Collins formula; sampling criteria

1. Introduction

Scalar diffraction theory has been widely used to simulate laser beam propagation, and is helpful in designing optical systems [1–4]. There are many methods to calculate the diffraction integrals, such as numerical integral method [1], angular spectrum method [5] and impulse response method [6]. The angular spectrum (AS) method is mainly based on the theory of Fourier optics [7], which can simulate field propagation with high accuracy in near field, but gives very noisy results in far field, and this severely limits its further applications. Some works [8–11] have been done to provide methods to extend the distance in which AS method can simulate field propagation with high accuracy. Matsushima and Shimobaba [9] propose a band-limited angular spectrum (BLAS) method where the bandwidth of the transfer function is limited to eliminate the frequency components which would cause aliasing. This method is equivalent to add a low pass filter to the transfer function. The distance where the simulation is of high accuracy in the BLAS method is longer than that in the traditional AS method. Nevertheless, the BLAS method still cannot give a satisfactory result in far field [10]. On the other hand, for the AS method, increasing the calculation window size is a general method to deal with the long-distance propagation [8], which will increase the sampling number greatly and cause a huge calculation burden. Xiao [10] puts forward a method that provides a larger calculation window size without increasing the calculation complexity, and this method gives good results from near field to far field. However, the method is only suited for free-space propagation. A general method is needed for simulating field propagation through paraxial optical systems with high accuracy.

In this paper, we present a wide-window angular spectrum (WWAS) method for simulating field propagation through paraxial optical systems represented by ABCD matrices. This method is based on the Collins formula and the scaled Fourier transform (SFT), and can sample the field in the input space, output space and spatial-frequency domains independently. And then, sampling criteria are also discussed. Finally, some numerical simulations are given to verify the correctness and the usefulness of our method.

2. Theory of WWAS method for ABCD systems

2.1. Scalar diffraction theory of ABCD systems

Collins [12] gives a link between the ray optics and the scalar diffraction theory to calculate field propagation through paraxial optical systems, and introduces the elements of ABCD ray matrices into the diffraction integral kernel. As a result of this, the diffraction integral is modified as:

$$\begin{aligned} U(x) &= \tfrac{1}{\sqrt{i\lambda B}} \int U(x_0) \times K(x_0, x) dx_0, \\ K(x_0, x) &= \exp\left[\tfrac{i\pi}{\lambda B}\left(Ax_0^2 - 2x_0 x + Dx^2\right)\right], \end{aligned} \tag{1}$$

where $U(x_0)$ and $U(x)$ are the input and output fields; λ denotes the wavelength; and A, B, D are ray matrix elements. The constant term, $\exp(i\pi z/\lambda)$, is omitted here because it has no effects on the distribution of the output

*Corresponding author. Email: liyuanyang1108@sina.com

field. There are only three matrix elements in Equation (1), and the fourth element C can be determined by applying one of the properties of the ray matrix: $AD\text{-}BC = 1$. The element B is located in the denominator in Equation (1), which would make the integral undefined when $B = 0$. The case of $B = 0$ makes the input and output planes conjugate, thus the field distribution would not change after propagation. It is not necessary to use any algorithms to simulate this case at all, so we ignore the situation of $B = 0$. Figure 1 presents the field propagation model described by Equation (1). For reasons of brevity, we concentrate on one-dimensional cases, and for two-dimensional cases, if there are no non-separable optical components, the generalization of our algorithm would be straightforward. However, if there is an optical component which cannot be represented by two independent ABCD matrices in X- and Y-directions at the same time, the discussions given here would not be sufficient enough.

Equation (1) can be rearranged into a more easily manipulated form where the integral kernel is written as

$$K(x_0, x) = \exp\left\{\frac{i\pi}{\lambda B}\left[(A-p)x_0^2 + p\left(x_0 - \frac{x}{p}\right)^2 + \left(D - \frac{1}{p}\right)x^2\right]\right\}. \tag{2}$$

We introduce a new parameter p in Equation (2). Substituting Equation (2) into Equation (1) and changing variable x to px, we can get

$$U(px) = \frac{1}{\sqrt{i\lambda B}}\exp\left[\frac{i\pi p^2}{\lambda B}\left(D - \frac{1}{p}\right)x^2\right] \times \int U(x_0)\exp\left[\frac{i\pi}{\lambda B}(A-p)x_0^2\right]\exp\left[\frac{i\pi p}{\lambda B}(x_0 - x)^2\right]dx_0. \tag{3}$$

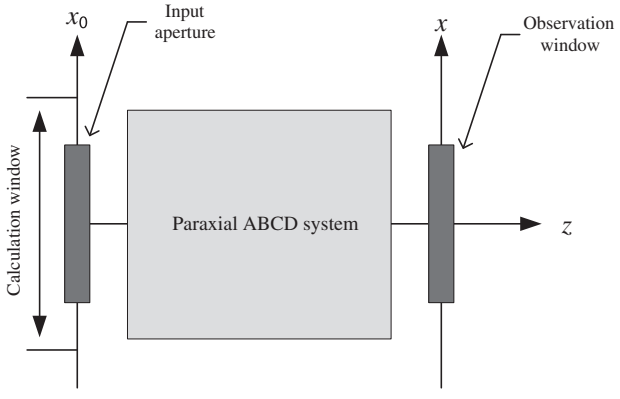

Figure 1. Model of the field propagation through optical systems.

Equation (3) is equivalent to Equation (1) except for the variable substitution, which can be explained as a coordinate scaling process. Now, it can be noticed that the new parameter p we introduced here has a physical meaning as a magnifying power which scales the output coordinate. In the mathematical sense, the parameter p can be chosen arbitrarily, but we will show it later that this parameter is still limited by the sampling criteria given in Section 3. Convolution theorem can be used due to the convolution form of Equation (3):

$$U(px) = \exp\left[\frac{i\pi p^2}{\lambda B}\left(D - \frac{1}{p}\right)x^2\right]F^{-1}\{A_0(u) \times H(u)\}(x), \tag{4}$$

where,

$$A_0(u) = F\left\{U(x)\exp\left[\frac{i\pi}{\lambda B}(A-p)x^2\right]\right\}(u), \tag{5}$$

$$H(u) = F\left\{\frac{1}{\sqrt{i\lambda B}}\exp\left(\frac{i\pi p}{\lambda B}x^2\right)\right\}(u) = \sqrt{\frac{1}{ip}}\exp\left(-i\pi\lambda\frac{B}{p}u^2\right). \tag{6}$$

F and F^1 are Fourier transform and its inverse, respectively. The procedure of traditional AS method can be used to calculate Equation (4): Firstly, $A_0(x)$ is computed using the fast Fourier transform algorithm (FFT). Secondly, $A_0(x)$ is multiplied by $H(u)$. Finally, the output field $U(x)$ is obtained after an inverse Fourier transform of $A_0(x) \times H(u)$. It is worth noting in Equation (5) that $A_0(x)$ is the angular spectrum of the product of the input field and a chirp function, instead of the input field only in traditional AS method.

Based on the traditional AS method, the transfer function of free-space propagation can be written as [9]

$$H_0(u) = \exp\left(-i\pi\lambda B u^2\right). \tag{7}$$

Equations (7) and (6) basically have the same form, which means that Equation (4) can be explained as a kind of free-space propagation whose model is shown in Figure 2. In Figure 2, the input field is modulated by an ideal lens whose focal length f is $B/(A-p)$ after passing through the input aperture. Then, the field propagates a distance of B/p in the free space. Finally, the output coordinate is scaled by the magnifying power p to get the final output field. Therefore, we change the field propagation through paraxial optical systems to a free-space propagation case, because of the equivalence between the models in Figures 1 and 2, which makes that some important conclusions in the free-space propagation case can be used in this study.

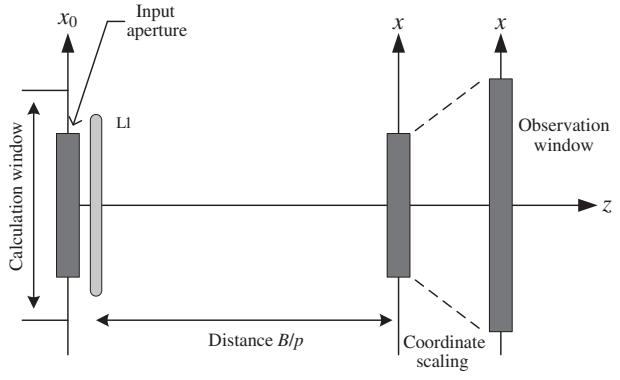

Figure 2. The equivalent model of Figure 1 based on Equation (4).

2.2. SFT with different sampling numbers in two domains

For the traditional Fourier transform, the sampling interval in the frequency domain equals to the reciprocal of the product of the sampling interval and sampling number in the input domain, while the sampling number in the frequency domain is the same as that in the input domain. This may bring difficulties in some situations. For example, if the sampling interval in the input domain is very small, it would become large in the frequency domain, and the large sampling interval in the frequency domain could induce the aliasing error [9]. The SFT [11] described in this section could be taken with different sampling intervals and sampling numbers in both domains, which relaxes the sampling condition for the traditional Fourier transform. We only discuss one-dimensional cases in this paper, and extension to two-dimensional cases is straightforward.

The input function is denoted as $f(x)$ here, and its SFT is given by

$$F_m^{\alpha} = \sum_{n=-N/2}^{N/2} f_n \exp\left(i2\pi \frac{\alpha nm}{N}\right), \tag{8}$$

where m and n run from $-M/2$ to $M/2-1$ and $-N/2$ to $N/2-1$, respectively. The symbol f_n denotes the sampled version of $f(x)$. The sampling numbers M and N could have different values. If the sampling interval of the input domain is denoted as δ and the sampling interval of the frequency domain is δ_M, the scale coefficient α equals to $\delta_M \times (N\delta)$. This means that the sampling interval δ_M in the frequency domain in this algorithm is α times larger (or smaller if $\alpha < 1$) than the one in a tradition discrete Fourier transform algorithm. The scale coefficient α must be located in the range of $[-N/M, N/M]$, otherwise aliasing error corrupts the result. If the scale coefficient α has a negative value, Equation (8) indicates an inverse Fourier transform. After some rearrangements of Equation (8), we have

$$F_m^{\alpha} = \exp\left(i\pi \frac{\alpha m^2}{N}\right) \sum_{n=-N/2}^{N/2} f_n \exp\left(i\pi \frac{\alpha n^2}{N}\right) \exp\left(-i\pi \frac{(n-m)^2}{N}\right). \tag{9}$$

Equation (9) has a convolution form, which means that we can apply the convolution theorem to it as:

$$F_m^{\alpha} = \exp\left(i\pi \frac{\alpha m^2}{N}\right) \mathrm{FFT}^{-1}\{\mathrm{FFT}\{\mathbf{g}\} \times \mathrm{FFT}\{\mathbf{h}\}\}, \tag{10}$$

where,

$$g_n = f_n \exp\left(i\pi \frac{\alpha n^2}{N}\right), \; h_n = \exp\left(-i\pi \frac{n^2}{N}\right). \tag{11}$$

FFT and FFT^{-1} are the fast Fourier transform algorithm and its inverse, respectively. The SFT can be obtained using two FFTs and an inverse FFT based on Equation (10). Note that FFT can calculate the circular convolution, but it cannot give directly the linear convolution. In order to use the circular convolution to calculate the linear one, we need to extend the vectors $\mathbf{g}$ and $\mathbf{h}$ as [9,13]

$$\begin{aligned} \mathbf{g} &= \{\underbrace{0,0,\ldots,0}_{M/2}, \underbrace{g_{-N/2}, g_{-N/2+1}, \ldots, g_{N/2-1}}_{N}, \underbrace{0,0,\ldots,0}_{M/2}\}, \\ \mathbf{h} &= \{\underbrace{h_{-(N+M)/2}, h_{-(N+M)/2+1}, \ldots, h_{(N+M)/2-1}}_{N+M}\}. \end{aligned} \tag{12}$$

The vectors are extended to $(N+M)$ elements in Equation (12), and the linear convolution is the central M elements of the consequential vector obtained by Equation (10). The WWAS method for paraxial optical systems will be discussed below using this SFT algorithm.

2.3. WWAS method for ABCD systems

The WWAS method is based on Equation (4) and the SFT algorithm. The SFT algorithm separates the sampling processes in the input space, spatial-frequency and output space domains. The flow chart of the WWAS method for ABCD systems is shown in Figure 3. Four steps, which are used to calculate field propagation through optical systems with the WWAS method, are discussed as follows:

(1) The basic parameters are decided primarily. In the input domain, the input field $U_1(x)$ is sampled within the input aperture which equals to

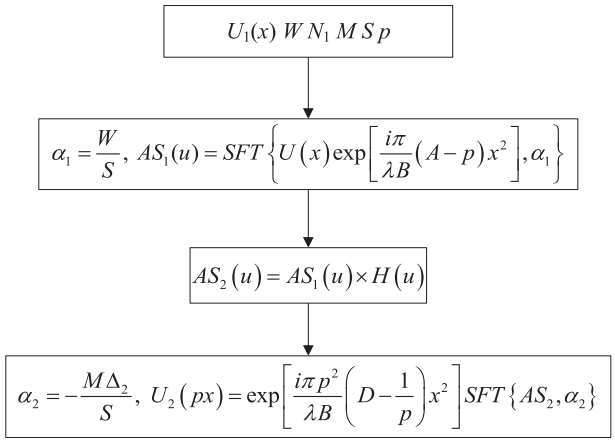

Figure 3. Schematic representation of the WWAS method for paraxial ABCD systems. The four blocks are schematic representations of the four steps, respectively.

the aperture of the paraxial optical system and has a size of W. The sampling number of the input aperture is N_1, thus the sampling interval Δ_1 is W/N_1. In the spatial-frequency domain, the sampling number is M, and the sampling interval Δ_u is $1/S$, where S is the calculation window size shown in Figure 2. Choosing the value of S is the most important issue in this algorithm, and it will be discussed in detail in Section 3. In the output domain, the size of the observation window is $p \times W$, which means that the observation window is p times larger (or smaller if $p < 1$) than the input aperture. The sampling interval in the output domain is $p \times \Delta_2$, and the sampling number is $N_2 = W/\Delta_2$. The parameters W, N_1, S, N_2 and p can be chosen independently, but they are limited by the sampling criteria that will be given in Section 3 below.

(2) The function $AS_1(u)$ in Figure 3 equals to the Fourier transform of the product of the input field $U_1(x)$ and the chirp function $\exp[i\pi/(\lambda B)(A-p)x^2]$. We name, for convenience, the function $AS_1(u)$ as the input angular spectrum, though the real input angular spectrum is the Fourier transform of the input field. The Fourier transform in this step is obtained by the SFT algorithm. The scale coefficient α_1 equals to W/S. The sampling number of $AS_1(u)$ is M and the interval is $1/S$, which have been given in the first step.

(3) The input angular spectrum is multiplied by the transfer function in Equation (6). The result, $AS_2(u)$, is named as the output angular spectrum.

(4) Finally, the output field $U_2(px)$ is obtained by the scaled inverse Fourier transform of $AS_2(u)$. In this step, the scale coefficient α_2 is $-M\Delta_2\Delta_u$. The parameter p in $U_2(px)$ means that the observation window size is p times as large as the input aperture size.

3. Discussion of sampling criteria

We cannot obtain a correct simulation unless the choices of the basic parameters fulfill the sampling criteria. For the WWAS method, the calculation window size S shown in Figure 2 has two functions, which are: (1) to decide the sampling interval of the frequency domain; and (2) to provide a guard band around the input aperture. The parameter S plays the most important role in the WWAS method, which is very different from other AS methods. Thus, in the following discussion of the sampling criteria, we mainly concentrate our attention on the parameter S.

3.1. *Sampling criterion of SFT*

The scale coefficient α_1 must be located in the region of $[-N_1/M, N_1/M]$ according to the discussion in Section 2.2. We have already known that the parameter N_1 denotes the sampling number in the input space domain, and that M denotes the sampling number in the spatial-frequency domain. Taking into account that α_1 equals to W/S, we can get

$$S \geq \frac{M}{N_1} W. \tag{13}$$

Equation (13) guarantees the correctness of the input angular spectrum. Likewise, the second scale coefficient α_2 is limited in $[-M/N_2, M/N_2]$ where N_2 denotes the sampling number of the output space domain. Considering that $\alpha_2 = -M\Delta_2\Delta_u$, an inequality is given by

$$S \geq W, \tag{14}$$

which guarantees the correctness of the output field calculated from the output angular spectrum. The two inequalities in Equations (13) and (14) are weak conditions unless the Fresnel number of the equivalent free-space propagation model in Figure 2 is very large.

3.2. *Physical sampling criterion*

This sampling criterion is determined not by a particular algorithm, but by the physical nature of field propagation. Note that the equivalent model in Figure 2 changes the problem of field propagation through ABCD systems to the free-space propagation problem, thus we only need to analyze the sampling criteria of the free-space

propagation here, which has been discussed in details in several researches [6,9,14], and we can use these conclusions directly.

The free-space propagation model is shown in Figure 4. The angular spectrum emitted from the edge of the input aperture must cover the whole observation window to avoid the loss of the spatial-frequency components. The maximum angular spectrum $u_{\max}$ is determined by the sampling number M and the sampling interval Δ_u in the spatial-frequency domain as

$$u_{\max} = \frac{M}{2} \cdot \Delta_u = \frac{M}{2S} = \frac{\sin\theta_m}{\lambda}, \tag{15}$$

where θ_m is the angle between the maximum angular spectrum and the z axis. In order to cover the whole observation window, we can derive an inequality from the geometry in Figure 4:

$$\sin\theta_m \geq \sin\theta = W\left[W^2 + (B/p)^2\right]^{1/2} \tag{16}$$

Taking Equation (16) into Equation (15), we have

$$S \leq \frac{\lambda M}{2W}\left[W^2 + (B/p)^2\right]^{1/2} \tag{17}$$

Equation (17) gives the upper boundary of the calculation window size S.

3.3. Sampling criterion for transfer functions

The transfer function $H(u)$ in Equation (6) is a chirp function whose phase is $\Phi(u) = -\pi\lambda B/pu^2$. In order to sample the chirp function correctly, the maximum change in the phase must be no more than π between any two adjacent sampling points [6], which yields

$$\Delta_u \left|\frac{\partial\Phi(u)}{\partial u}\right|_{u_{\max}} \leq \pi. \tag{18}$$

Taking $\Phi(u)$ into Equation (18) yields

$$u_{\max} \leq \frac{pS}{2\lambda B}. \tag{19}$$

Equation (19) reveals the upper boundary of the spatial-frequency, which means that the bandwidth of the spatial-frequency is limited due to the sampling criterion of the transfer function.

The sampling of the input field would result in the replicas of the calculation window as shown in Figure 4. If the aliasing spectrum emitted from the replicated windows propagates into the observation window, it would cause aliasing error. A larger calculation window size S can provide more guard band area to protect the observation window from the aliasing spectrum. The smallest value of S is determined by the maximum angular spectrum according to Figure 4 as

$$S \geq W + \frac{B}{p}\tan\theta_m. \tag{20}$$

Equation (19) can be substituted by a stronger condition which is

$$u_{\max} = \frac{\sin\theta_m}{\lambda} \leq \frac{\tan\theta_m}{\lambda} \leq \frac{pS}{2\lambda B}. \tag{21}$$

Taking Equation (21) into Equation (20), we have

$$S \geq 2W. \tag{22}$$

This means that, under the condition of Equation (21), if the calculation window size S is twice larger than the input aperture size, there would be no aliasing error caused by the replicas of the calculation window. Considering that $u_{\max} = M/(2S)$, the rearrangement of Equation (21) can be presented by

$$S \geq \frac{1}{2\sqrt{2}p}\left[\lambda^2M^2p^2 + \left(\lambda^4M^4p^4 + 64\lambda^2p^2B^2M^2\right)^{1/2}\right]^{1/2}. \tag{23}$$

3.4. Synthesis of the sampling criteria

Since Equations (13), (22) and (23) limit the lower boundary of S simultaneously, we have to introduce the following inequality to make sure that all the three equations keep correct at the same time:

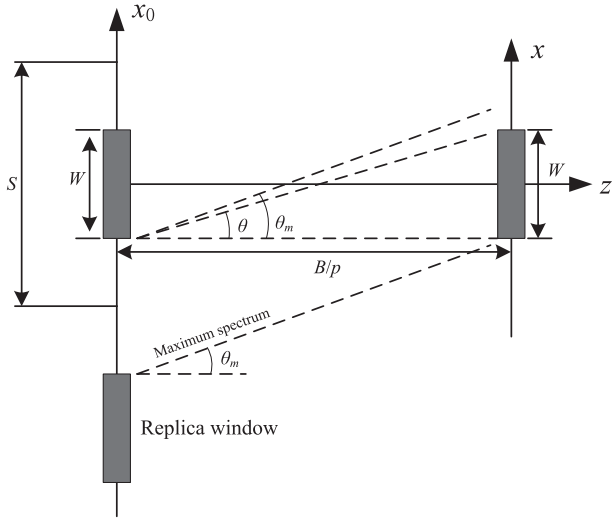

Figure 4. The geometry of the free-space propagation model.

$$\frac{1}{2\sqrt{2}p}\left[\lambda^2M^2p^2+\left(\lambda^4M^4p^4+64\lambda^2p^2B^2M^2\right)^{1/2}\right]^{1/2} \geq \max\{2W, MW/N_1\}. \tag{24}$$

We can find that Equation (24) gives a limit of the magnifying power p, but it is too complex to be presented analytically. We need to do some approximation that: if the propagation distance is far greater than the input aperture size, the value of θ_m would be very small, thus we have $\sin\theta_m \approx \tan\theta_m$. This would result in

$$\frac{1}{2\sqrt{2}p}\left[\lambda^2M^2p^2+\left(\lambda^4M^4p^4+64\lambda^2p^2B^2M^2\right)^{1/2}\right]^{1/2} \approx \sqrt{\frac{\lambda MB}{p}}. \tag{25}$$

Applying Equation (25), the rearrangement of Equation (24) yields

$$p \leq \min\left\{\frac{\lambda BN_1^2}{MW^2}, \frac{\lambda BM}{4W^2}\right\}, \tag{26}$$

which is a simplified version of Equation (24). Equation (26) is clearer than Equation (24) to demonstrate an upper limit of the magnifying power p. However, it is worth to remember that Equation (26) is an approximate result, and gives a larger range than the one predicted by Equation (24), if the condition of this approximation is not satisfied. If the propagation distance is not far greater than the input aperture, we should take a smaller range than the one Equation (26) predicted, and then check whether it satisfies Equation (24).

Above all, when Equation (24) (or Equation (26)) is satisfied, the limitation of the calculation window size S is defined by Equations (17) and (23) as

$$\frac{1}{2\sqrt{2}p}\left[\lambda^2M^2p^2+\left(\lambda^4M^4p^4+64\lambda^2p^2B^2M^2\right)^{1/2}\right]^{1/2} \leq S \leq \frac{\lambda M}{2W}\left[W^2+(B/p)^2\right]^{1/2}. \tag{27}$$

Hence, Equation (24) (or Equation (26) under the approximation) and Equation (27) are the sampling criteria of the WWAS method for beam propagation through paraxial optical systems.

Table 1. Elements of the matrix for simulation.

A	B (mm)	C (mm^{-1})	D
−0.0487	106.2910	−0.0095	0.1818

4. Numerical calculation and application

4.1. Simulations for a paraxial optical system

The optical system for simulation is a laser beam focusing system, which can focus a beam on a target of 500 mm away from the last component of the system. The specific structure of this system is not important, because we can describe it by an ABCD ray matrix if there is no vignetting. The matrix of the whole optical system can be obtained by multiplying all the matrices of single components in sequence [1], which is shown in Table. 1.

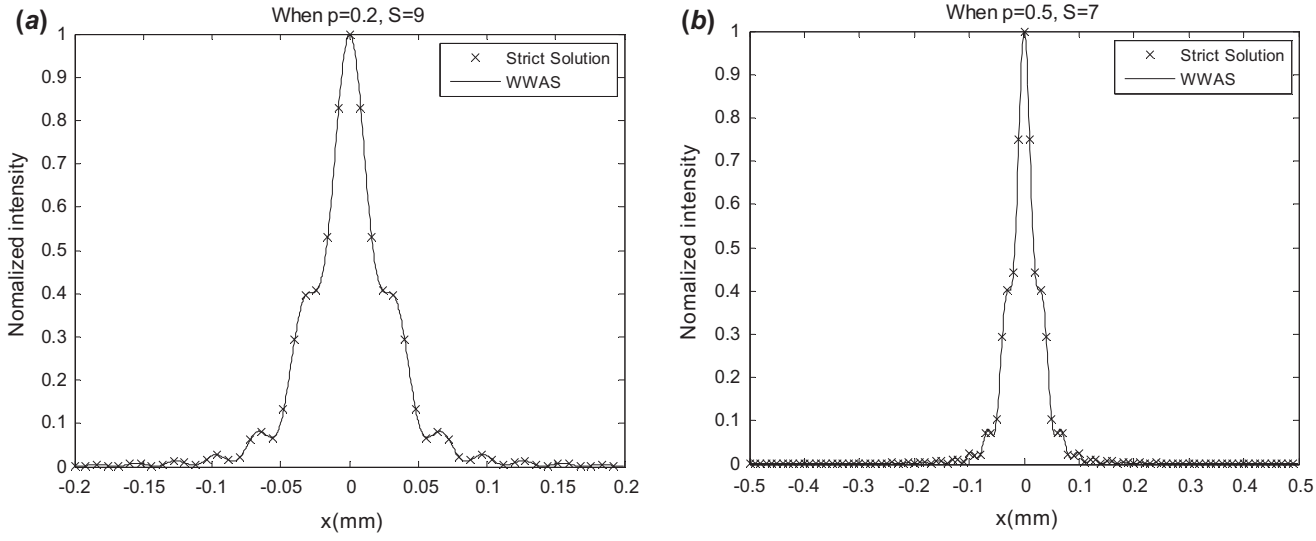

Figure 5. The results of the WWAS method for the paraxial optical system and the strict solutions calculated using the numerical integral method.

In this section, all the simulations are examined by the strict solutions computed using Equation (1) with the numerical integral method. We require that the input field is a plane wave, and its wavelength is 0.532 μm. The input aperture width W is set to be 2 mm, and the sampling numbers of the input aperture (input space domain), the spatial-frequency domain and the observation window (output space domain) are $N_1 = 256$, $M = 512$, $N_2 = 1024$, respectively. Note that the sampling numbers of the three domains can be set as different values, which is one of the advantages of our method. In this situation, the maximum value of the magnifying power p can be evaluated using Equation (26), which turns out to be 1.81. For this reason, we could find a certain range of S if the value of p is smaller than 1.81. If we set the magnifying power as $p = 0.2$, then the size of the observation window can be derived by $p \times W = 0.4$ mm. Taking all the parameters into Equation (27), we have a range of S as $6.02\,W \le S \le 18.1\,W$. When S takes the value of 9 W, the result of the WWAS method is shown in Figure 5(*a*), which is consistent with the strict solution exactly. If we increase p from 0.2 to 0.5, the observation window size becomes 1 mm, and Equation (27) then suggests that the range of S is $3.8\,W \le S \le 7.24\,W$. This time, if we make $S = 7\,W$, the result shown in Figure 5(*b*) is still consistent with the strict solution well, and we get a larger observation window than that in Figure 5(*a*) due to the larger value of the magnifying power p.

We can treat the simulation error as a kind of noise since they all make the results deviating from a strict

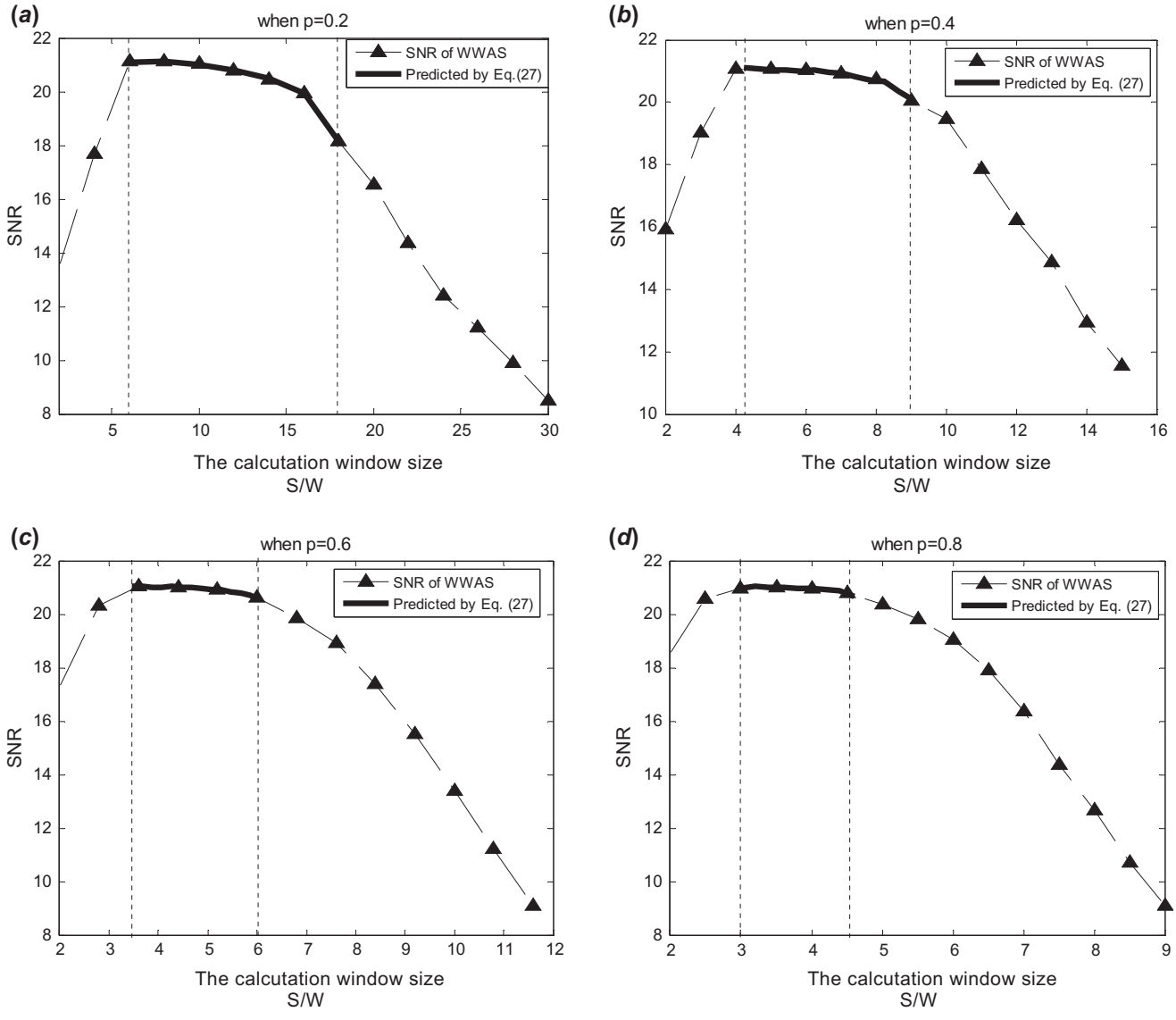

Figure 6. The SNRs as the functions of the calculation window size S.

one. Therefore, the concept of signal-to-noise ratio (SNR) in the field of signal processing is appropriate to measure the deviation of the simulation from the strict solution. The SNR is defined as [10]

$$\mathrm{SNR} = 10\lg\frac{\int_{\infty} I(x)dx}{\int_{\infty} |I(x) - I_N(x)|dx}, \tag{28}$$

where $I(x)$ is the result of the WWAS method and $I_N(x)$ is the strict solution calculated by numerical integral. The SNRs are shown in Figure 6 as functions of the calculation window size S, when the magnification p has different values. The parts of the curves between two vertical dot lines are the predicted ranges of Equation (27). When $p = 0.2$, 0.4, 0.6 and 0.8, the ranges predicted by Equation (27) have the relatively high SNRs as shown in Figure 6, which means that Equation (27) is a correct criterion for the WWAS method. It is interesting to notice that the highest SNR value always appears near the lower boundary of Equation (27). In the range determined by Equation (27), a larger value of parameter S results in a simulation with lower SNR. Comparing the four cases in Figure 6, we can also find that the decrease of the SNRs is somehow affected by the magnifying power p, and we will give our explanation for this fact next.

We find that the error of the upper boundary of Equation (27), when p is small, comes from the plane wave nature of the angular spectrum. Figures 7(*a*) and (*b*) show the simulations when p is set to be 0.1. The predicted range of Equation (27) is from 8.5 to 36.2 *W*. When the parameter S equals to 8.5 *W*, the result of the

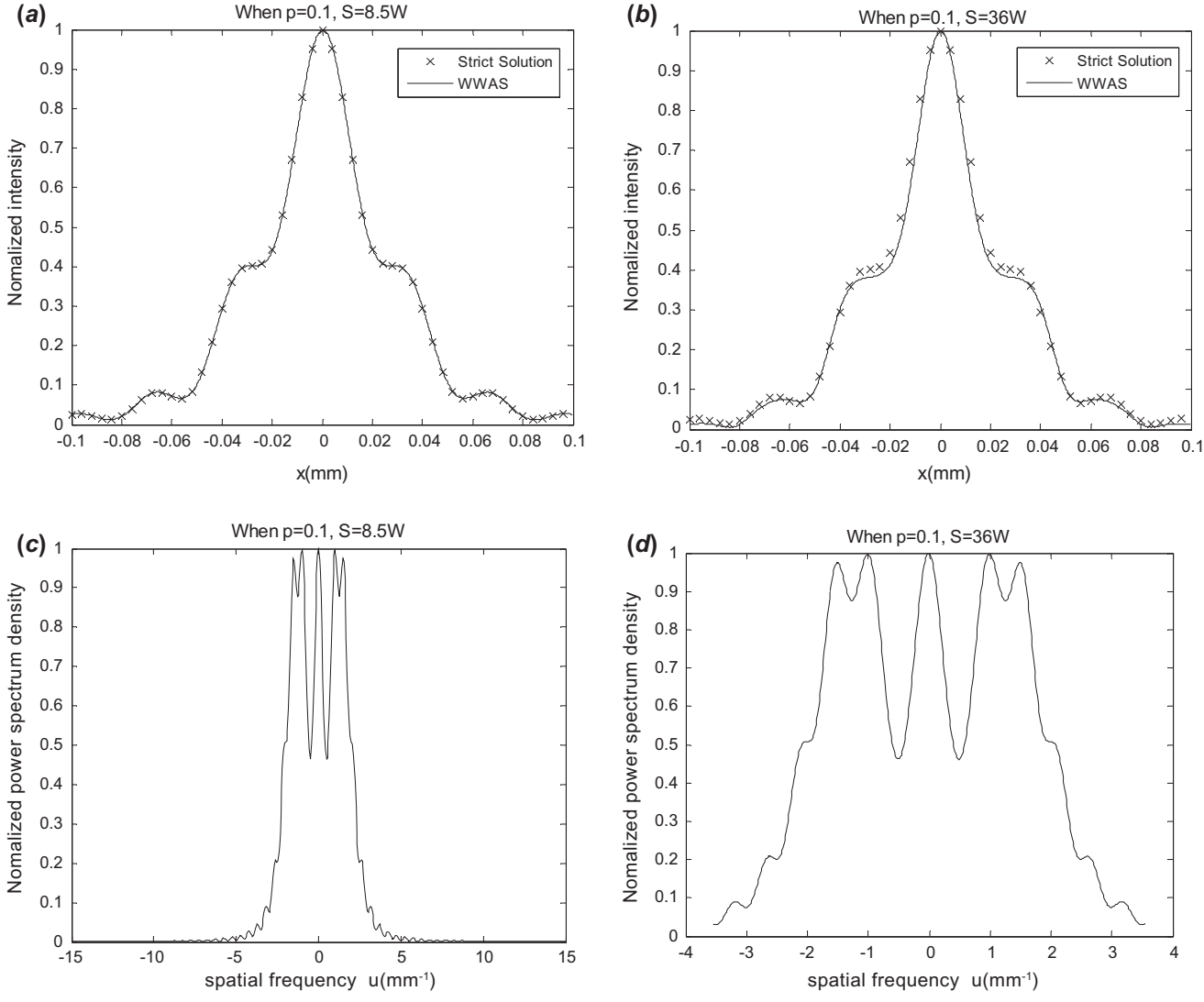

Figure 7. The accuracy of the WWAS algorithm when S is the lower and upper boundaries of Equation (27). (*a*) and (*b*) are the intensity distributions. (*c*) and (*d*) are the power spectrum densities of the spatial-frequency.

WWAS method in Figure 7(*a*) is exactly the same as the strict solution. However, in Figure 7(*b*), when $S = 36\,W$, which is near the upper boundary of Equation (27), the result of the WWAS method contends significant error, which is what we have mentioned in Figure 6. The power spectrum density of the input field is shown in Figures 7(*c*) and (*d*), and we can find that the power spectrum density is truncated by the calculation window in Figure 7(*d*). Based on the derivation of Equation (17), the lost part of the power spectrum density would not affect the simulation in the observation window, which is true if we treat the angular spectrum as rays [9]. However, if we consider the plane wave nature of the angular spectrum, each plane wave (angular spectrum) contributes to the modulation of the field in the observation plane at a particular frequency. If some angular spectrum is truncated, the field would lose some frequency components, which causes the error in Figure 7(*b*). Therefore, the error of the upper boundary of Equation (27) comes from the simplified ray model of angular spectrum and it is impossible to avoid it. What we can do is to make the value of S approach to lower boundary of Equation (27), so as to avoid the truncating error of the angular spectrum when p is small.

4.2 *Simulations for free-space propagation*

There are some advantages in applying our algorithm in the free-space propagation. It is difficult for the traditional AS method and the BLAS method, an improved version of traditional AS method, to simulate the long-distance propagation, because sampling the transfer function becomes harder when the propagation distance is great [6]. The WWAS method for free space

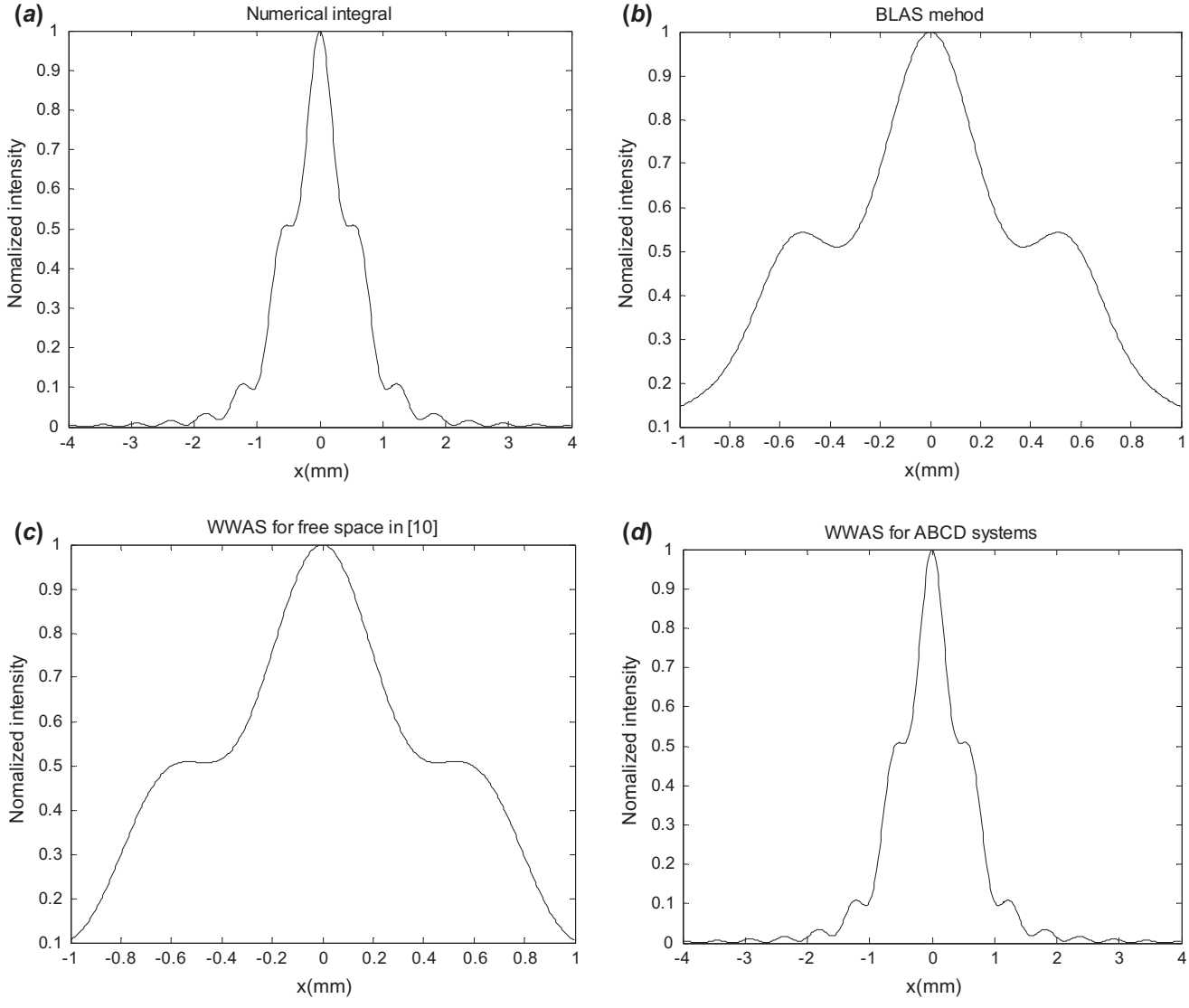

Figure 8. The simulations of the free-space propagation using different AS methods when the propagation distance is 2000 mm.

in [10] is an excellent work to extend the high accurate range of the BLAS method from near to far field. However, the observation window has the same size as the input aperture in this method, thus we can only observe part of the distribution of the optical field. Next, we will show that all the disadvantages of the three AS methods can be overcome by our algorithm

For the free-space propagation, the matrix elements A and D have unit values, while C equals to zero and B is the propagation distance. The input field is a plane wave with a wavelength of 0.532 μm, and the input aperture size W is set to be 2 mm. The sampling numbers of the input aperture, the spatial-frequency domain and the observation window are all 512. The simulations are shown in Figure 8 using four kinds of different methods when the propagation distance B is 2000 mm. Figure 8(a) is the result of numerical integral which we take as a strict solution. The result of BLAS method is shown in Figure 8(b), which is a wrong outcome due to the false sampling of the transfer function. The result in Figure 8(c) is calculated by the WWAS method for free-space propagation discussed in [10]. It is correct with high accuracy, but the observation window is too small to provide a whole picture of the intensity distribution. Figure 8(d) is the result of our WWAS method for ABCD systems when $p = 4$ and $S = 8$. This result shows that the WWAS method for ABCD systems not only has the high accuracy for long-distance propagation, but also has enough observation window size. If we want to get the same effect using the method in [10], we have to increase the input aperture size and the sampling number, which may cause huge calculation burdens. However, we can use our WWAS method for ABCD systems to accomplish this work without increasing the sampling burden.

5. Conclusion

The WWAS method is developed to simulate optical field propagation through ABCD systems. Using the Collins formula, we obtain an equivalent free-space propagation model, instead of the tradition model which has ABCD systems inside. This equivalence is very useful, as it changes the field propagation through paraxial optical systems to the free-space propagation. Hence, we can use some valuable conclusions of the free-space propagation directly, which simplifies the discussion of the sampling criteria.

We use a SFT to take the place of the traditional Fourier transform in this method. The SFT has different sampling intervals and sampling numbers in the input and frequency domains. Using the SFT, we accomplish the independent samplings of the input space domain, the spatial-frequency domain and the output space domain, which is important for the WWAS method, since we can choose the parameter S in the spatial-frequency domain without affecting the sampling parameters in other domains.

We discuss the sampling criteria from three aspects: the sampling criteria of the SFT, the physical nature and the transfer function. Then, we synthesis all the sampling criteria and obtain Equation (24) (or Equation (26) for approximation) and Equation (27) as the sampling criteria of the WWAS method for ABCD systems.

The numerical simulations of an optical system and a free-space propagation case are discussed. We prove the WWAS method and its sampling criteria correct with the simulations of the optical system given in Table 1. We point out that the error of the upper boundary of Equation (27) comes from the plane wave nature of the angular spectrum, so the parameter S should be set near the lower boundary when p is small. In the simulations for the free space, we find that the WWAS method for ABCD systems in this paper has higher accuracy in the long-distance propagation than the BLAS method, and unlike the method in [10], our method can get enough observation window size without increasing the sampling burden.

Funding

This work was supported by the Funds of the State Key Laboratory of Laser Interaction with Matter of China.

References

[1] Siegman, A.E. *Lasers;* University Science Books, Mill Valley, CA, 1986.
[2] Carter, W.H. *Appl. Opt.* **1982,** *21,* 1989–1994.
[3] Yura, H.T.; Hanson, S.G. *J. Opt. Soc. Am. A* **1987,** *4,* 1931–1948.
[4] Mei, Z.; Zhao, D.; Wei, X.; Jing, F.; Zhu, Q. *Optik* **2005,** *116,* 521–526.
[5] Voelz, D.G. *Computational fourier Optics: A matlab tutorial;* SPIE, Bellingham, WA, 2011.
[6] Voelz, D.G.; Roggemann, M.C. *Appl Opt* **2009,** *48,* 6132–6142.
[7] Goodman, J.W. *Introduction to Fourier Optics;* McGraw-Hill, New York, NY, 1996.
[8] Liu, J.P. *J. Opt. Soc. Am. A* **2012,** *29,* 1956–1964.
[9] Matsushima, K.; Shimobaba, T. *Opt. Express* **2009,** *17,* 19662–19673.
[10] Xiao, Y.; Tang, X.; Peng, H.; Wang, W. *Opt. Lett.* **2012,** *37,* 4943–4945.
[11] Nascov, V.; Logofătu, P.C. *Appl. Opt.* **2009,** *48,* 4310–4319.
[12] Collins, S.A. Jr *JOSA* **1970,** *60,* 1168–1177.
[13] Oppenheim, A.V.; Schafer, R.W. *Digital Signal Processing;* Prentice-Hall, New Jersey, NJ, 1975.
[14] Coy, S. In *Choosing Mesh Spacings and Mesh Dimensions for Wave Optics Simulation*, Advanced Wavefront Control: Methods, Devices, and Applications III, San Diego, CA, USA, Jul 31–Aug 2, 2005; SPIE: San Diego, CA, 2005; pp 1–12.